Article

Soluble αβ-tubulins reversibly sequester TTC5 to regulate tubulin mRNA decay

Alina Batiuk [1], Markus Höpfler [2], Ana C. Almeida [1], Deryn Teoh En-Jie [3], Oscar Vadas [4], Evangelia Vartholomaiou [1], Ramanujan S. Hegde [2], Zhewang Lin [3] ✉ & Ivana Gasic [1] ✉

Microtubules, built from heterodimers of α- and β-tubulins, control cell shape, mediate intracellular transport, and power cell division. The concentration of αβ-tubulins is tightly controlled through a posttranscriptional mechanism involving selective and regulated degradation of tubulin-encoding mRNAs. Degradation is initiated by TTC5, which recognizes tubulin-synthesizing ribosomes and recruits downstream effectors to trigger mRNA deadenylation. Here, we investigate how cells regulate TTC5 activity. Biochemical and structural proteomic approaches reveal that under normal conditions, soluble αβ-tubulins bind to and sequester TTC5, preventing it from engaging nascent tubulins at translating ribosomes. We identify the flexible C-terminal tail of TTC5 as a molecular switch, toggling between soluble αβ-tubulin-bound and nascent tubulin-bound states. Loss of sequestration by soluble αβ-tubulins constitutively activates TTC5, leading to diminished tubulin mRNA levels and compromised microtubule-dependent chromosome segregation during cell division. Our findings provide a paradigm for how cells regulate the activity of a specificity factor to adapt posttranscriptional regulation of gene expression to cellular needs.

Built from heterodimers comprising α- and β-tubulin proteins (αβ-tubulins hereafter), microtubules are core eukaryotic cytoskeletal elements[1]. Cells rely on microtubules for the organization of their internal contents, motility, and division[2]. To execute their roles effectively, cells must tightly regulate the spatial distribution and dynamic properties of microtubules[3], achieved through numerous regulatory pathways. Foremost among these is microtubule dynamic instability manifested in consecutive phases of growth through the addition, and shrinkage through the loss of αβ-tubulins[4]. By regulating dynamic instability through microtubule and tubulin-binding proteins[5,6], cells can use microtubule growth and shrinkage to power various physical processes such as chromosome segregation during cell division.

Microtubule dynamics are critically dependent on the concentration of soluble αβ-tubulins. As their core building blocks, soluble αβ-tubulins directly impact microtubule nucleation, polymerization,

and dynamic properties[7,8]. Cells therefore tightly regulate the availability of soluble αβ-tubulins through a feedback loop that restricts the biosynthesis of new tubulin when αβ-tubulins are in surplus[9,10]. Termed tubulin autoregulation, this pathway involves the selective degradation of tubulin-encoding mRNAs in a translation-dependent reaction[9,11–13]. The mechanism involves a ribosome-binding factor termed TTC5 (tetratricopeptide protein 5), which selectively recognizes the N-terminal sequences of nascent α- and β-tubulins at the ribosomal exit tunnel[14]. TTC5 recruits the adaptor protein SCAPER (S-Phase Cyclin A Associated Protein in the ER), which recruits the large deadenylase complex CCR4-NOT (Carbon Catabolite Repression–Negative On TATA-less), initiating tubulin mRNA deadenylation and decay[15].

In cells, various physiological and toxic stimuli can destabilize microtubules, leading to an increase in the proportion of soluble

[1]Department of Molecular and Cellular Biology, University of Geneva, Geneva, Switzerland. [2]Medical Research Council Laboratory of Molecular Biology, Cambridge, UK. [3]Department of Biological Sciences, National University of Singapore, Singapore, Singapore. [4]Proteins, Peptides and RNA to Protein Core Facility, Faculty of Medicine, University of Geneva, Geneva, Switzerland. ✉e-mail: zlin@nus.edu.sg; ivana.gasic@unige.ch

αβ-tubulins and initiating tubulin autoregulation[16,17]. Experimentally, this can be replicated using several microtubule-depolymerizing agents, such as colchicine, nocodazole, or combretastatin A4[9,14,15,18]. Although the precise signal generated by the rise in soluble αβ-tubulins that triggers tubulin autoregulation is yet to be identified, both qualitative and quantitative changes are known to occur when microtubules depolymerize into soluble αβ-tubulins. These changes include posttranslational modifications, such as tyrosination and ubiquitination, and interactions with specific binding partners, such as stathmin and CLIP-170[5,19]. Additionally, depolymerization presumably renders αβ-tubulins accessible to degradation machineries[20,21].

Mutations in TTC5 or SCAPER associated with complete or near-complete loss of protein have been linked to tubulinopathies—a class of neurodevelopmental disorders arising from mutations in tubulins[22–27]. Disruption of tubulin autoregulation in cultured cells compromises mitotic fidelity[14,15], a phenotype frequently attributed to aberrant microtubule dynamics[28,29]. This phenotype is seen with mutations that perturb TTC5 recognition of the ribosome, recognition of nascent tubulins, recruitment of SCAPER, or SCAPER-mediated recruitment of CCR4-NOT[14,15]. Thus, the ribosome-proximal molecular events in tubulin autoregulation that culminate in mRNA decay are now generally well established[14,15]. By contrast, the mechanisms that control the deployment of this mRNA decay machinery remain unknown. In this study, we focus on how cells control the activity of TTC5, which serves as both the specificity factor and the most upstream component of ribosome-associated mRNA decay[14,15].

Results

Soluble αβ-tubulins can directly inhibit TTC5 activity

TTC5 binding to tubulin-synthesizing ribosomes initiates tubulin mRNA decay[14]. Because tubulin mRNA degradation is thought to be modulated by the cell in response to perceived tubulin need, we speculated that TTC5 abundance, localization, or engagement of ribosome-nascent chain complexes (RNCs) is likely to be regulated (Fig. 1a). Immunoblotting showed that TTC5 protein levels remain constant before and after acute microtubule destabilization by colchicine (COL), combretastatin A4 (CA4), or nocodazole (NOC, Fig. S1a), each of which triggers tubulin mRNA degradation[9,16]. Furthermore, a model where microtubule-sequestered TTC5 is released upon depolymerization seems unlikely because GFP-TTC5 (fully competent for tubulin autoregulation[15]) is diffusely cytosolic without an obvious microtubule localized population (Fig. S1b). Finally, simply overexpressing TTC5 in cells is insufficient to trigger tubulin mRNA degradation (Fig. S1c, d) unless the autoregulation pathway is triggered by microtubule destabilization[14]. These results suggest that TTC5 is constitutively present in the cytosol, but does not initiate tubulin mRNA degradation under normal steady-state conditions.

Previously, cytosol extracted from untreated cells, but not colchicine-treated cells, was proposed to contain an inhibitor of TTC5 activity[14]. In this experiment, an in vitro assembled complex between TTC5 and tubulin-synthesizing RNCs could be disrupted by cytosol from cells growing under normal conditions but not from cells undergoing active tubulin mRNA decay induced by colchicine treatment[14]. Speculating that this putative inhibitory factor might act directly on TTC5, we used recombinant immobilized TTC5 to identify interaction partners from the cytosol of untreated vs colchicine-treated TTC5 knockout cells. The only differentially interacting protein recovered stoichiometrically with TTC5 from untreated cell lysates was identified by mass spectrometry as a stoichiometric mixture of α- and β-tubulins (Figs. 1b and S1e).

Because the cell lysates were prepared on ice, both the untreated and colchicine-treated cytosol had equal amounts of depolymerized αβ-tubulin heterodimers, with little or no intact microtubules (whose polymerization is temperature-dependent[30,31]). Indeed, no appreciable

TTC5 co-sedimented with polymerized purified porcine brain αβ-tubulins (Fig. 1c), consistent with an absence of GFP-TTC5 co-localization with microtubules in cells (Fig. S1b). By contrast, in an in vitro assay soluble porcine brain αβ-tubulins interacted with recombinant TTC5 with a Kd of ~0.5 μM (Fig. S1f, S1g) and progressively inhibited TTC5-RNC interaction with an estimated Ki of ~0.5 μM (Fig. 1d). Thus, soluble αβ-tubulins at physiological concentrations (1–3 μM) are direct competitors of RNCs for binding to TTC5.

TTC5 inhibition by αβ-tubulins is attenuated during autoregulation

The capacity of soluble αβ-tubulins to bind immobilized TTC5 was progressively lost over the course of 60 min when cells were pre-treated with colchicine prior to preparation of cytosol (Fig. 1e). Importantly, post-lysis addition of colchicine to cytosol prepared from untreated cells had no effect on the αβ-tubulin-TTC5 interaction (Fig. 1e, lane 2). Similarly, purified porcine αβ-tubulins showed no difference in their TTC5 interaction regardless of any pre-incubation with colchicine (Fig. S1h, lane 2). Thus, colchicine treatment of live cells, but not cytosol or purified tubulins, triggers a yet-unidentified signal that changes the capacity of soluble αβ-tubulins to interact with TTC5. This loss of interaction with αβ-tubulins is a downstream consequence of microtubule disruption and correlates with the disappearance of a TTC5-inhibitory activity in the cytosol as monitored using in vitro assays, and further correlates with the initiation of tubulin mRNA decay in cells[9].

Colchicine-triggered loss of a TTC5 sequestration factor was further supported by the finding that recombinant TTC5 could selectively pulldown tubulin-encoding mRNAs from the cytosol of colchicine-pretreated TTC5 knockout cells (Figs. 1f and S1i). Roughly six- to eight-fold less tubulin mRNA was pulled down by TTC5 from the cytosol of untreated cells or cytosol treated with colchicine after cell lysis. Notably, the 60 min time course of colchicine-triggered tubulin mRNA recovery by TTC5 mirrored the loss of interaction between αβ-tubulins and TTC5 (Fig. 1e). Total tubulin mRNA levels remained unchanged throughout these treatments as expected for TTC5 knockout cells (Fig. S1j). A similar colchicine-triggered shift of TTC5 interaction partners was seen in proteomic analysis of GFP-TTC5 pulldowns before and after colchicine treatment. Here, we observed a markedly reduced recovery of multiple TTC5 interactors, including several tubulin isotypes, and an increased recovery of ribosomal proteins and SCAPER upon treatment with colchicine (Fig. S1k, l). Manual annotation based on the conservation, subcellular location, ubiquitous expression, and abundance, revealed tubulins as the only possible TTC5 sequestration factors. Similar losses of TTC5-tubulin interactions were seen with nocodazole-mediated microtubule destabilization (Fig. S1m). As expected, paclitaxel-mediated (PTX) microtubule stabilization—previously reported to stabilize tubulin mRNAs[9,16,17]—did not trigger TTC5 dissociation from αβ-tubulins (Fig. S1m, n). These data further support a model where a yet unidentified upstream signal generated by an increase in soluble αβ-tubulin abundance initiates tubulin autoregulation.

To directly monitor the autoregulation-triggered disruption of the tubulin-TTC5 interaction in living cells, we carried out proximity labeling using the promiscuous biotin ligase TurboID fused to TTC5 and expressed at near-endogenous levels (Fig. S1o). Quantitative mass spectrometry of biotinylated proteins revealed that tubulins were strongly proximal to TTC5 in untreated cells but substantially less in cells treated with colchicine (Fig. 1g and S1p, q). Thus, TTC5 is engaged with soluble αβ-tubulins in cells and in vitro. The clear anti-correlation of the αβ-tubulin-TTC5 interaction vs the capacity of TTC5 to engage tubulin-synthesizing RNCs and initiate mRNA decay argues that soluble αβ-tubulins are potent repressors of TTC5 activity. This repressive interaction is progressively lost upon conditions that trigger tubulin mRNA decay, indicating that a key control point in tubulin
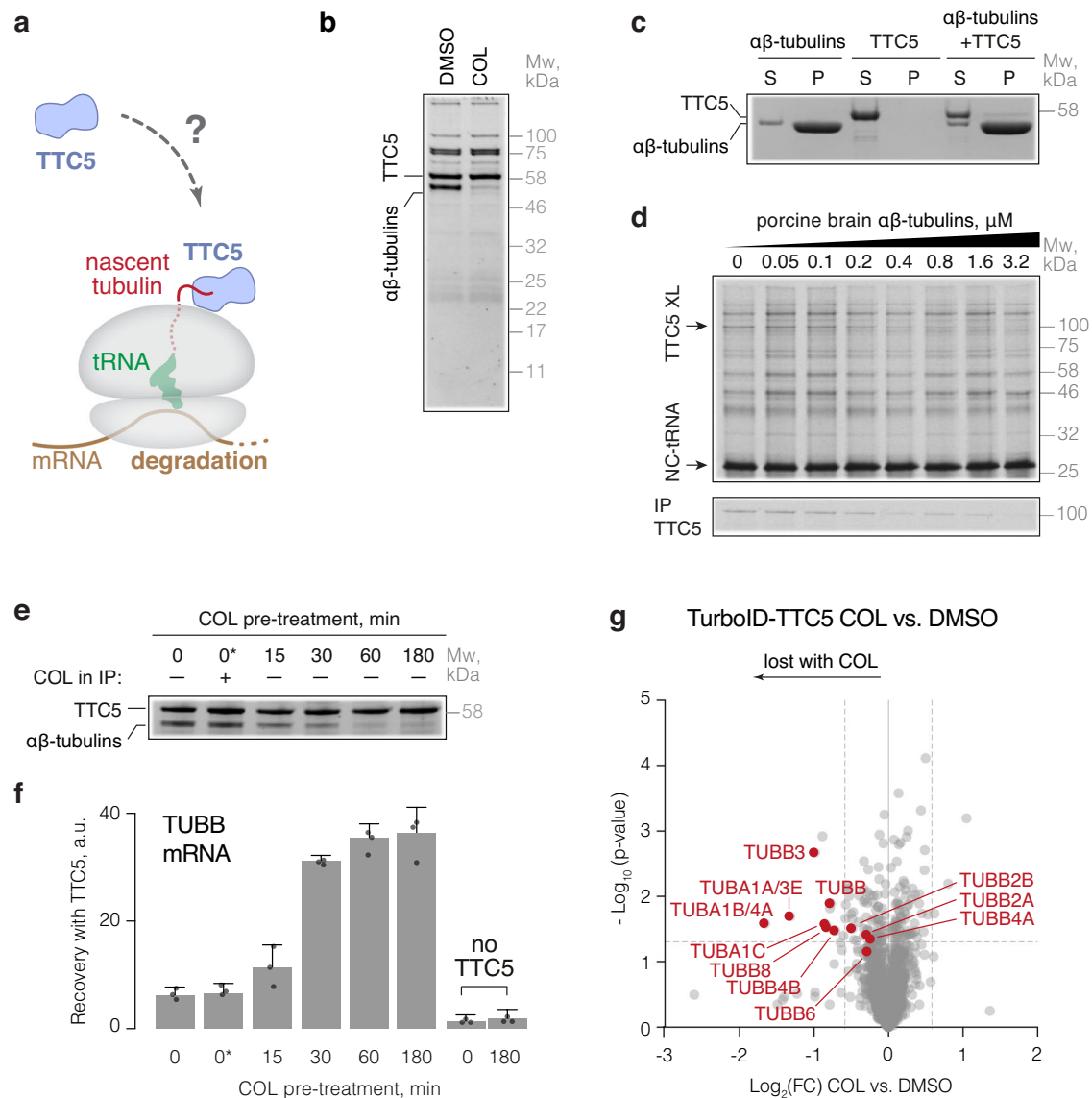
Fig. 1 | Soluble αβ-tubulins reversibly repress TTC5 to regulate its activity.
a The tubulin autoregulation pathway. **b** Recombinant Strep-tagged TTC5 was mixed with lysate from untreated or colchicine-treated (COL, 3 h) TTC5 knockout HEK293 cells and recovered by affinity purification via the Strep-tag. The sole differential interaction partner was a mixture of αβ-tubulins. Depicted is a representative blot from three independent experiments. **c** Binding of TTC5 to microtubules was analyzed by microtubule co-pelleting assay. Representative blot from three independent replicates is shown. TTC5 mostly remains in the soluble fraction (S), while microtubules are mostly in the pellet (P). **d** Nascent β-tubulin crosslinking assay in the presence of the indicated concentrations of soluble porcine brain αβ-tubulins. The TTC5 crosslink is indicated and verified by immuno-precipitation (bottom panel). The 94-residue β-tubulin nascent chain was produced in rabbit reticulocyte lysate in the presence of ^{35}S-methionine and the UV-activated cross-linking amino acid p-benzoyl-L-phenylalanine (Bpa) was incorporated at position 7 by amber suppression. Ribosome-nascent chain complexes were isolated and incubated with porcine brain tubulin and cross-linked under UV light.

Reactions were immuno-precipitated with anti-TTC5 antibody or analyzed by SDS-PAGE and autoradiography. Shown is a representative blot from three independent replicates. **e** TTC5 knockout HEK293 cells were pre-treated for the indicated times with colchicine, and then lysed. One aliquot of each lysate was used for binding analysis to recombinant Strep-TTC5 as in (**b**). One control sample included colchicine added after cell lysis (indicated as 0*). Depicted is a representative blot from three independent replicates. **f** The products coimmunoprecipitated with recombinant TTC5 in panel (**e**) were analyzed for α- (Fig. S1i) and β-tubulin mRNAs by quantitative RT-PCR (mean ± SD from three independent replicates) and normalized to a reference transcript (RPLP1). **g** Proximity labeling using TurboID fused to TTC5 and expressed in TTC5 knockout HEK293 cells, followed by enrichment of biotinylated proteins and quantitative mass spectrometry. Data from cells treated with colchicine were normalized to DMSO control and plotted as Log$_2$ fold-change (Log$_2$(FC)). Dashed lines represent a threshold of 1.5-fold change and 0.05 p-value. Annotated are different tubulin isoforms. Processed data are provided in Supplementary Data 1. Source data for this figure are provided as a Source Data file.

autoregulation is the reversible sequestration of TTC5 by soluble αβ-tubulins.

The C-terminal tail of TTC5 acts as a molecular switch
To identify TTC5 domains required for repression by αβ-tubulins, we used hydrogen–deuterium exchange-based structural mass spectrometry (HDX-MS). In HDX-MS experiments, amide-bond hydrogens in dynamic regions of proteins are exchanged for deuterium, which can be monitored by mass spectrometry[32]. TTC5 in isolation showed high deuteration in loops connecting alpha-helices of its tetratricopeptide repeats, and a near complete deuteration in its ~20 amino acid C-terminal tail (Figs. 2a–c and S2a), suggesting that this
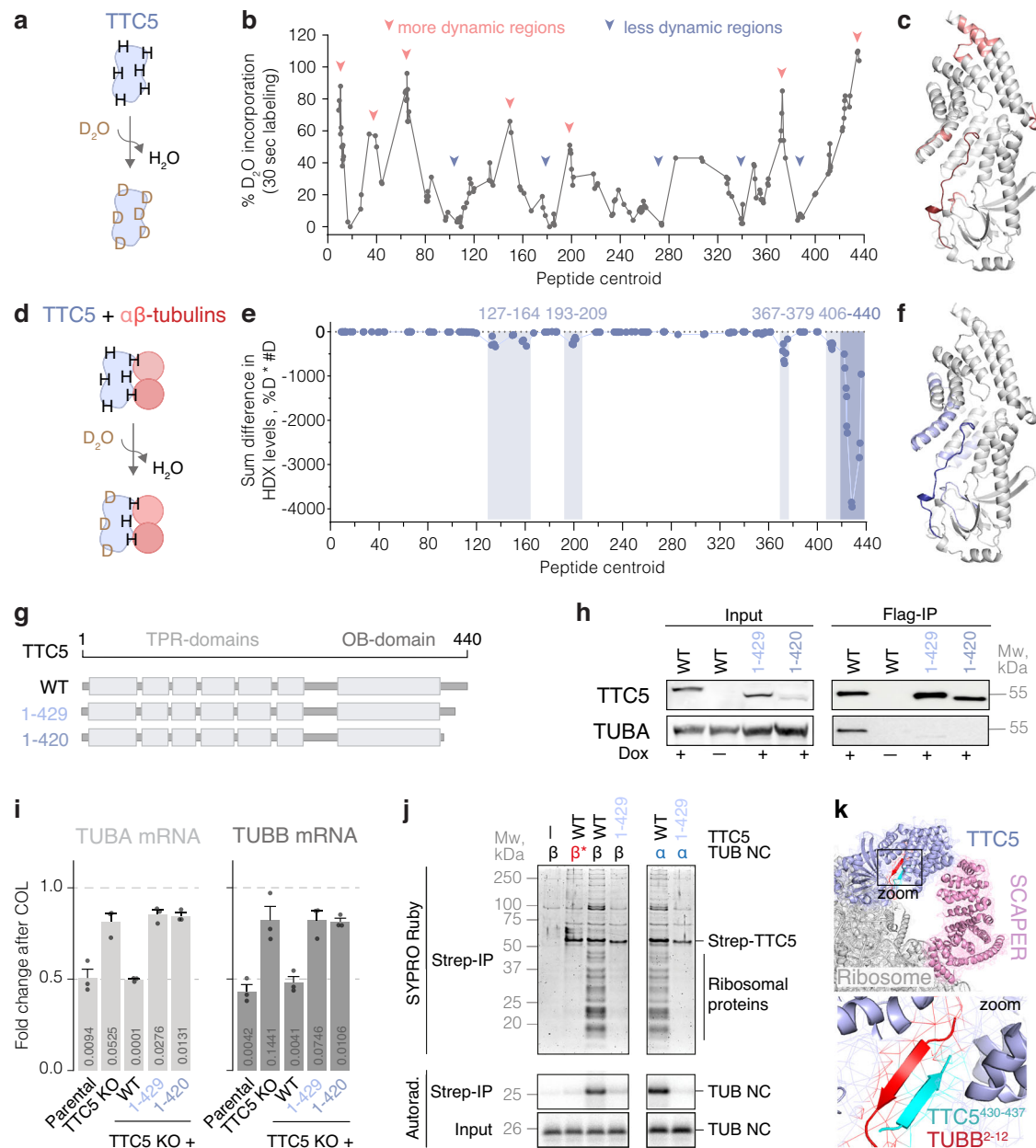
Fig. 2 | C-terminal tail mediates interaction with mature and nascent tubulin.
a HDX-MS approach. **b** Deuteration profile of human recombinant Strep-TTC5 identifies the C-terminal domain as highly flexible or dynamic. Data are represented as means over three independent replicates. **c** Deuteration profile mapped onto the AlphaFold2-predicted structure of human TTC5 (AF-Q8N0Z6-F1)[33]. **d** HDX-MS approach. **e** Differential deuteration profile of human recombinant Strep-TTC5 upon incubation with porcine brain tubulin for 5 min. Data are presented as a sum of differences in hydrogen/deuterium exchange (% deuterons × number of deuterons) in the TTC5 + αβ-tubulins vs TTC5 alone samples in three independent replicates. Shaded areas highlight regions on TTC5 that show significantly lower deuteration upon binding to αβ-tubulin. **f** Differential deuteration profile mapped onto the AlphaFold2-predicted structure of human TTC5. **g** Schematic representation of the generated TTC5 constructs. **h** Indicated Flag-tagged TTC5 constructs were expressed in HeLa TTC5 knockout cells and affinity purified via the Flag tag. Coimmunoprecipitated interactors were separated using SDS-PAGE and tubulins were visualized using western blot. The experiment was repeated three times with similar results. **i** Autoregulation assay with HeLa parental, TTC5 knockout, and the indicated Flag-TTC5 rescue cell lines. Data show the mean ± SD mRNA levels after colchicine treatment from three independent experiments. Indicated are p-values in unpaired, two-tailed Student's t-test for each of the cell lines with the DMSO-treated sample as reference. **j** Sixty-four-residue α- and β-tubulin nascent chains (TUB NC) were produced in rabbit reticulocyte lysates in the presence of ^{35}S-methionine and recombinant wild-type (WT) or mutated Strep-TTC5. Strep-TTC5 and its associated proteins were subsequently enriched via the Strep-tag and visualized by SYPRO Ruby staining and autoradiography. β* indicates a β-tubulin construct in which its TTC5-interacting N-terminal MREI motif has been mutated to autoregulation-incompatible MHQV[14]. The data shown is from a single experiment, which was confirmed by data obtained through orthogonal methods (Fig. 2i, k). **k** Close-up view of the AlphaFold2-predicted C-terminal domain of TTC5 (cyan) and nascent β-tubulin (red) forming a beta-sheet, fitted into the experimental cryo-EM density from a recent study (PDB: 8BPO)[15]. Source data for this figure are provided as a Source Data file.

region is devoid of secondary structure elements. Of these deuterated sites, only the C-terminal tail (residues ~420–440) showed marked protection from deuteration in the presence of αβ-tubulins. Modest but specific reductions in deuteration were also seen at residues 127–164, 193–209, and 367–379, regions that are all on the same face of TTC5 (Figs. 2d–f and S2b). These observations suggest that TTC5 interaction with αβ-tubulins buries or otherwise alters these regions of TTC5, particularly its C-terminal tail.

The TTC5 C-terminal tail is required for its interaction with αβ-tubulins as seen in pulldown experiments with two truncated TTC5 mutants, TTC5[1-429] and TTC5[1-420] (Fig. 2g, h). Similar results were obtained in cells using proximity labeling. Immunostaining for biotinylated proteins revealed that tubulins were substantially less biotinylated in TTC5 KO cells re-expressing TurboID fused to either TTC5[1-429] or TTC5[1-420] compared to wild-type TTC5 (Fig. S2c). In the absence of sequestration by αβ-tubulins, TTC5[1-429] or TTC5[1-420] were expected to constitutively engage tubulin RNCs and trigger tubulin mRNA decay. In fact, TTC5[1-429] and TTC5[1-420] re-expressed in TTC5 knockout cells failed to degrade tubulin mRNA even upon colchicine stimulation (Figs. 2i and S2d), suggesting that TTC5's C-terminal tail has a functional role in mRNA decay.

To identify the step where the C-terminal tail plays a role, we analyzed TTC5 interaction with in vitro-produced RNCs of α- or β-tubulins. TTC5[1-429] was unable to effectively recover tubulin RNCs in a pulldown assay (Fig. 2j), indicating that the C-terminal tail is critical for the recognition of tubulin-synthesizing RNCs. This was surprising because this tail was not modeled in the initial cryo-electron microscopy (cryo-EM) structure of tubulin RNCs engaged by TTC5[14]. An AlphaFold2[33] multimer prediction with full-length TTC5 and the N-terminal region of β-tubulin showed the C-terminal tail of TTC5 (residues 431–436) forming an anti-parallel beta-sheet with residues 4–8 in nascent β-tubulin, both of which are housed in TTC5's substrate-binding groove (Fig. S2e, f). We then re-inspected the improved cryo-EM map from a more recent study[15] and found that the density in the binding groove is consistent with a two-stranded beta-sheet (Figs. 2k and S2e, g). The snug fit of the N- and C-terminal tails of nascent tubulin and TTC5, respectively, into TTC5's groove, appears to be important for the stable association of TTC5 with tubulin-translating ribosomes.

Taken together, these results identify the flexible and unstructured C-terminal tail as having a critical role in two independent steps of the tubulin autoregulation pathway. Under steady-state conditions, this tail engages with and stabilizes an interaction between TTC5 and αβ-tubulins in a repressive complex. Although the molecular details of this interaction will require structural analysis, a direct role for the C-terminal tail is supported by both HDX-MS and the observed consequences of its deletion in vitro and in cells. Under autoregulation conditions, the same C-terminal tail forms a complex with nascent tubulin inside the binding groove of TTC5 at the ribosome. Thus, TTC5's C-terminal tail acts as a molecular switch, toggling between a repressive complex with soluble αβ-tubulins and an activated complex with nascent tubulin on the ribosome.

Loss of binding to αβ-tubulins constitutively activates TTC5

The N-terminal segment of nascent α-tubulin or β-tubulin engaged by TTC5 on the ribosome is buried in αβ-tubulins[34]. This suggests that, although the C-terminal tail of TTC5 is involved in both interactions, the molecular details are likely to differ. Furthermore, the TTC5 interaction with αβ-tubulins probably involves other regions of TTC5 as indicated by the HDX-MS results. We, therefore, reasoned that it might be possible to identify TTC5 mutants that lack its repressive interaction with αβ-tubulin while preserving its activity on tubulin-translating ribosomes. Such a mutant would allow us to test the biological importance of the repressive interaction with αβ-tubulin directly and specifically.

Focusing first on the C-terminal tail we found that mutating V430 and T432 to glutamic acid (TTC5[VTEE]) resulted in near complete loss of binding to αβ-tubulins (Fig. 3a, b). T432E alone was sufficient to mostly recapitulate this binding defect with αβ-tubulins as seen in pulldowns from cells (Fig. 3a, b). In a second approach, we deployed ConSurf[35], a tool that maps conservation onto the experimental structures of proteins. This analysis identified various conserved surface residues in TTC5 (Fig. S3a), which we mutated and found by pulldown that

TTC5[D175A] was markedly reduced in its ability to bind αβ-tubulin (Figs. 3b and S3b).

TTC5[D175A] and TTC5[T432E] were analyzed for their ability to interact with αβ-tubulins in live cells using bimolecular fluorescence complementation (BiFC)[36–38]. In these experiments, the N-terminal fragment of the yellow fluorescent protein (Venus[1–172], VN) was appended to TTC5, and the C-terminal fragment of the yellow fluorescent protein (Venus[156–238], VC) was fused to α- (TUBA1B) or β-tubulin (TUBB, Figs. 3c and S3c). The two fragment-fused proteins were stably expressed at equal levels in TTC5 KO cells from a single tandem open reading frame separated with a self-cleaving peptide (P2A). Both TTC5[D175A] and TTC5[T432E] BiFC constructs showed reduced fluorescence intensity relative to wild-type TTC5 when paired with either α- or β-tubulin (Figs. 3d, e and S3d, e). The expression levels of TTC5 mutants were comparable to wild-type TTC5, indicating that the reduced fluorescence signal was due to reduced interaction (Fig. S3f). Similar conclusions were reached from proximity-labeling assays, where TurboID ligase fused to the TTC5 mutants biotinylated tubulins less effectively than wild-type TTC5 (Fig. S3g).

In contrast to the interaction with αβ-tubulins, the TTC5 mutants were mostly competent for the engagement of tubulin-synthesizing RNCs produced by in vitro translation. In this experiment, immunoprecipitation via tagged recombinant TTC5 followed by visualization of ribosomal proteins revealed that TTC5[D175A] clearly engaged α- and β-tubulin RNCs, albeit somewhat less well than wild-type TTC5 (Figs. 3f and S3h). TTC5[T432E] showed unimpaired engagement of β-tubulin RNCs but partial impairment for α-tubulin RNCs compared to wild-type TTC5 (Fig. 3f). Thus, these mutants are mostly selective in their inability to be sequestered by αβ-tubulins, while still retaining their capacity to engage tubulin-synthesizing ribosomes.

When introduced into TTC5 knockout cells, both TTC5[D175A] and TTC5[T432E] showed markedly reduced baseline tubulin mRNA levels despite unaffected transcription as evidenced by unchanged levels of unspliced pre-mRNAs (Figs. 3g and S3i). These data are consistent with constitutive activation of the TTC5 mutant in the absence of efficient repression via αβ-tubulins. Interestingly, cells expressing these mutants still responded to colchicine treatment with further degradation of tubulin mRNAs (Figs. 3h and S3j). This might be due to a weak but still relevant binding of the TTC5 mutants to αβ-tubulins that is further lost upon colchicine, or could hint at another colchicine-regulated factor such as SCAPER. This remains to be investigated. Regardless, the data illustrate that point mutants that relatively selectively impair the TTC5 interaction with αβ-tubulins result in loosened regulation of tubulin mRNA degradation. We therefore conclude that αβ-tubulins are physiologically relevant regulators of TTC5 activity.

Constitutive activation of TTC5 causes mitotic defects

To investigate the physiological importance of αβ-tubulin-mediated repression of TTC5 in conditions that do not require chemical perturbation of the microtubule network, we leveraged the constitutively active TTC5 mutants, TTC5[D175A] and TTC5[T432E], and assessed mitotic fidelity in living cells using microscopy (Fig. 4a). In agreement with previous reports[14,15], compared to parental cells, TTC5 knockout cells showed a higher rate of errors in chromosome alignment onto the metaphase plate (2.8-fold, Figs. 4b and S4a), a higher rate of chromosome segregation errors in anaphase (2.6-fold, Figs. 4c and S4a), and a subtle but highly reproducible delay in mitotic progression (Fig. S4b). These phenotypes were rescued by re-expression of TTC5[WT]. Notably, the reconstitution of TTC5 KO cells with the constitutively active TTC5[D175A] and TTC5[T432E] mutants showed similar types and frequencies of errors as in the knockout cells (Figs. 4b, c and S4a–c). Thus, both the absence of TTC5-mediated autoregulation, which results in moderately higher tubulin mRNA than normal[15], and constitutively active TTC5, which results in
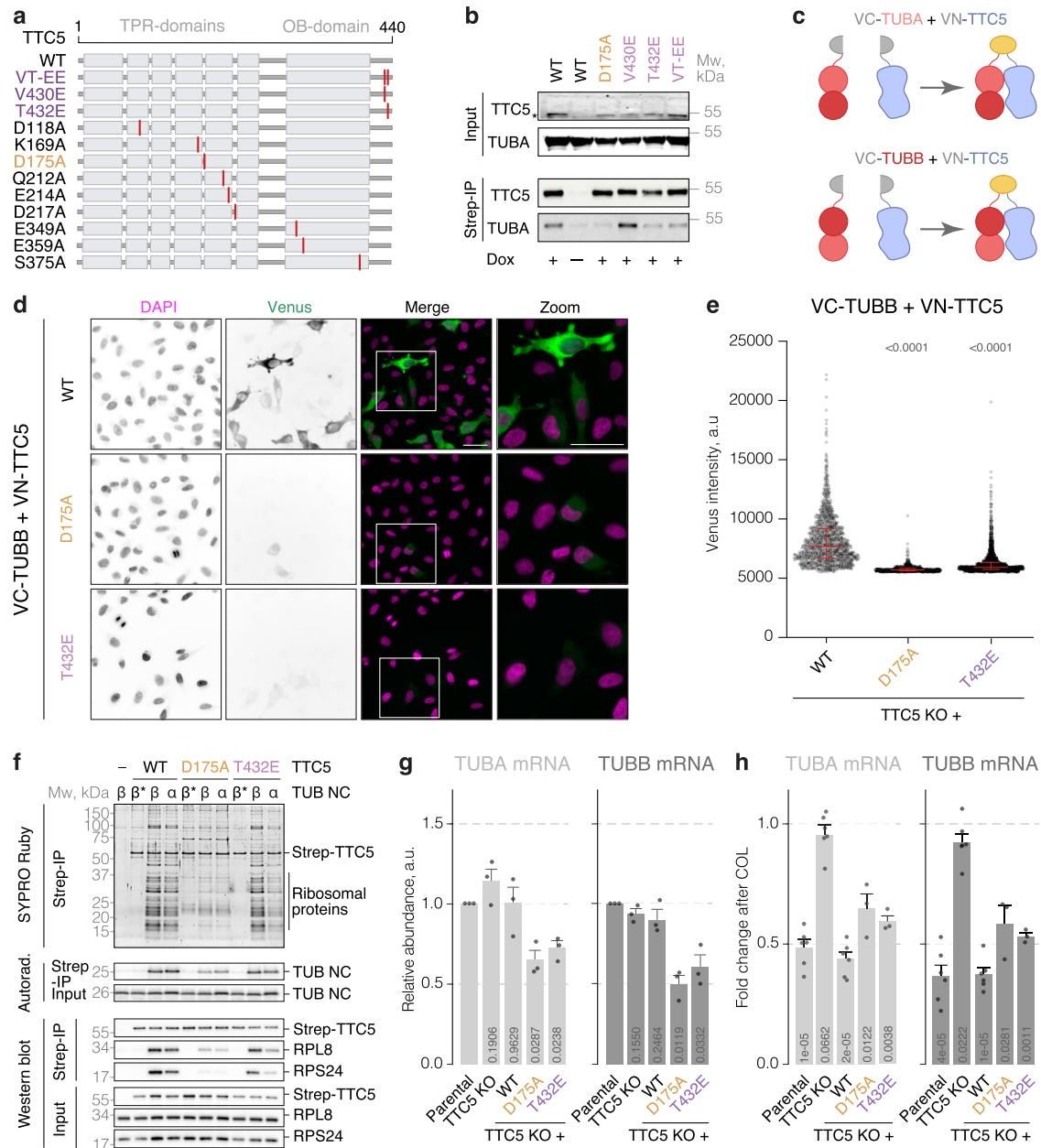
Fig. 3 | Loss of binding to αβ-tubulins constitutively activates TTC5.
a Generated TTC5 constructs. **b** Indicated Strep-TTC5 constructs were expressed in HeLa TTC5 knockout cells and pulled down via Strep-tag. Bound αβ-tubulins were visualized by western blot. The asterisk indicates Strep-TTC5. The experiment was repeated three times with similar results. **c** BiFC approach. **d** Representative images of the indicated constructs expressed in HeLa TTC5 knockout cells. Scale bar = 20 µm. **e** Fluorescence intensity of Venus across the indicated BiFC cell lines. Red lines depict median and interquartile fluorescence intensities. Indicated are p-values in the two-sided Mann–Whitney test for each of the BiFC constructs with the one based on TTC5^WT as reference. The experiment was done with six biological replicates, analyzing 6465, 2005, and 5258 cells for WT, D175A, and T432E samples, respectively. **f** Sixty-four-residue α- and β-tubulin nascent chains (TUB NC) were produced in rabbit reticulocyte lysates in the presence of ^{35}S-methionine and recombinant WT or mutated Strep-TTC5. Strep-TTC5 and its associated proteins were subsequently enriched via the Strep-tag. Interacting partners were visualized

by SYPRO Ruby staining, western blot, and autoradiography. β* indicates a β-tubulin construct in which its TTC5-interacting MREI motif has been mutated to autoregulation-incompatible MHQV. Data shown is representative of two replicate experiments for the D175A mutant, and from one experiment for the T432E mutant. Results were confirmed by orthogonal means (Fig. 3h). **g** Relative α- and β-tubulin mRNA levels in HeLa parental, TTC5 knockout, and the indicated Strep-TTC5 cell lines, normalized to a housekeeping transcript and the parental cell line. Data show the mean ± SD from three independent experiments. Indicated are p-values in unpaired, two-tailed Student's t-tests for each of the indicated cell lines with the parental cell line as reference. **h** Autoregulation assay with HeLa parental, TTC5 knockout, and the indicated Strep-TTC5 cell lines. Data show the mean ± SD mRNA levels from three (D175A and T432E) and six (Parental, TTC5 KO and WT) independent experiments. Indicated are p-values in unpaired, two-tailed Student's t-tests for each of the indicated cell lines with the DMSO-treated sample as reference. Source data for this figure are provided as a Source Data file.

lower tubulin mRNA than normal, impair mitotic fidelity. These results underscore the importance of maintaining tubulin mRNA levels within a specific and narrow range via a fully functional dynamic autoregulation system.

Discussion

Tubulin autoregulation was discovered over four decades ago, yet the control mechanisms governing it have long remained enigmatic. Early studies delineated the co-translational nature of this pathway and its
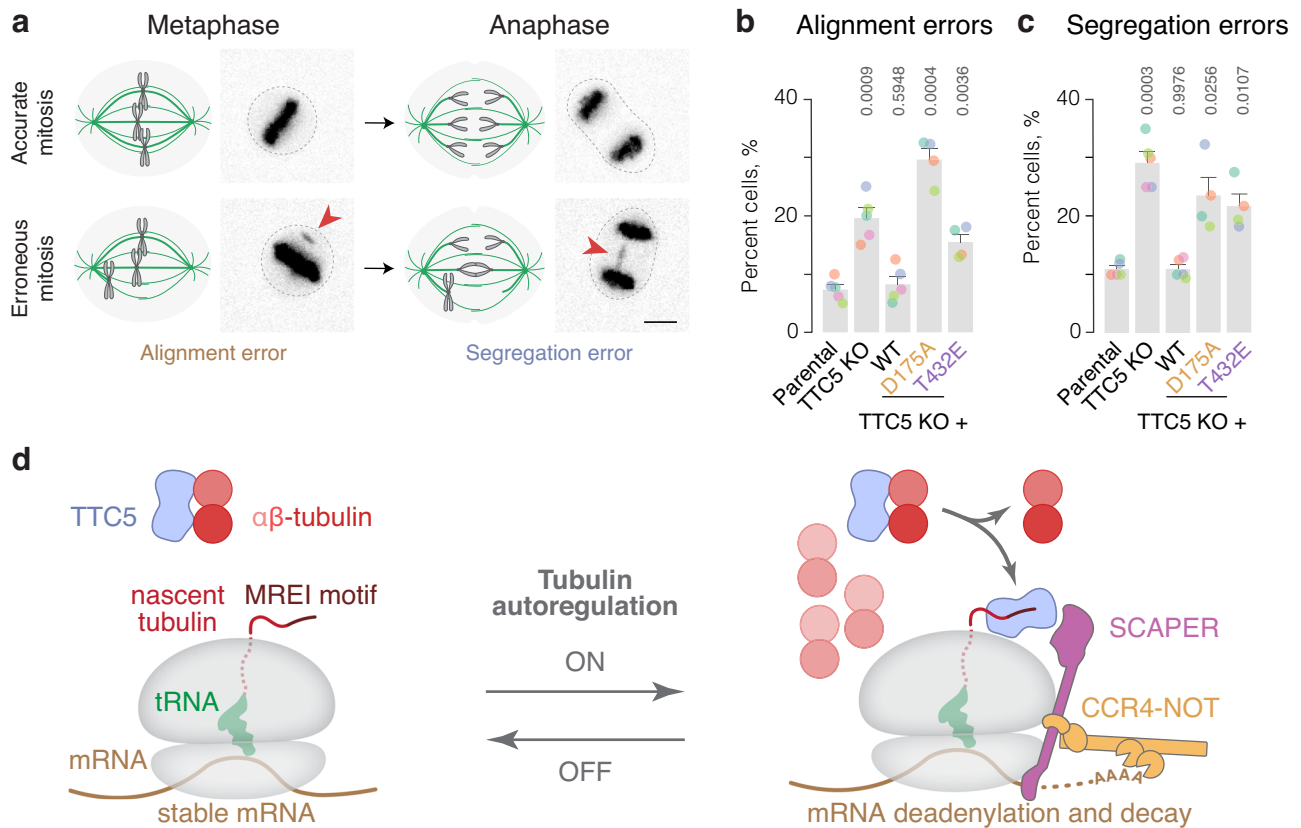
Fig. 4 | Constitutive activation of TTC5 causes mitotic defects. a Schematic and representative images of errors in chromosome alignment onto the metaphase plate and segregation in anaphase. Scale bar = 5 μm. **b, c** Occurrence of errors in chromosome alignment onto the metaphase plate (**b**) and errors in chromosome segregation in anaphase (**c**) in HeLa parental, TTC5 knockout, and the indicated Flag-TTC5 rescue cell lines. Data are presented as mean ± SD from three (D175A (101 cells) and T432E (134 cells)) or five (Parental (154 cells), TTC5 KO (140 cells), and WT (132 cells)) independent replicates represented with color-coded dots. Indicated are *p*-values in unpaired, two-tailed Student's *t*-tests for each of the indicated cell lines with the parental cell line as reference. **d** Proposed model for tubulin autoregulation. Source data for this figure are provided as a Source Data file.

sensitivity to microtubule depolymerizing drugs[9,11–13,39,40]. Recent investigations have elucidated the molecular players proximal to the ribosome, leading to a model where TTC5 engagement of nascent tubulin initiates a cascade involving SCAPER and the CCR4-NOT deadenylase complex, culminating in tubulin mRNA degradation[14,15]. Because this cascade is not constitutively active, one or more of its components must be under regulatory control to allow selective and dynamic activation of tubulin mRNA decay. These control point(s) have long been unclear, but are now amenable to study via TTC5, SCAPER, and CCR4-NOT.

Our study uncovers a crucial regulatory step in this pathway of selective mRNA decay: the reversible sequestration of TTC5 by soluble αβ-tubulins mediated by a previously overlooked C-terminal domain of TTC5. Under normal conditions, soluble αβ-tubulins sequester TTC5, preventing its engagement with RNCs (Fig. 4d). Given a Kd of 0.5 μM between αβ-tubulin and TTC5, roughly 85% of TTC5 (~35 nM in cells) would be sequestered by the ~3 μM soluble αβ-tubulin. The remainder (~5 nM) may be responsible for the low-level constitutive turnover of tubulin mRNA, explaining why TTC5 knockout cells have modestly elevated tubulin mRNA levels even in unperturbed conditions at steady state[15].

Upon microtubule destabilization, αβ-tubulins progressively lose their capacity to interact with TTC5, allowing TTC5 to engage tubulin-translating ribosomes and trigger mRNA degradation (Fig. 4d). Because the loss of interaction can be recapitulated using recombinant immobilized TTC5 in pulldown assays, we speculate that some change to αβ-tubulins triggered by microtubule depolymerization is responsible. Furthermore, the loss of interaction occurs progressively over 30–60 min and cannot be recapitulated with depolymerizing drugs in vitro. One explanation is a model where posttranslational modification(s) on αβ-tubulins progressively change, reducing their affinity to TTC5. Such posttranslational modifications would have to be reversible and occur on both the pre-existing and newly depolymerized tubulins to allow tubulin-translating ribosomes to gain a competitive advantage for TTC5. The observed 15 to 60 min timeframe required for TTC5 to translocate from αβ-tubulins to tubulin-translating ribosomes (Fig. 1e, f) may reflect the time required to posttranslationally modify a large pool of unpolymerized αβ-tubulins. Alternatively, or concomitantly, other proteins with higher affinity for soluble αβ-tubulins may become available and outcompete TTC5. Given the high complexity of the tubulin gene network[41], vast tubulin posttranslational modifications[42], and regulatory interaction partners[5], the possibilities are myriad. An important future goal is to elucidate the mechanism that controls the interaction between TTC5 and αβ-tubulins.

The fact that TTC5's C-terminal tail is involved in both its interaction with αβ-tubulins and with tubulin-synthesizing ribosomes is noteworthy. It helps explain why the two interactions seem to be mutually exclusive, and adds to our understanding of how the N-terminus of nascent tubulins is recognized. A combination of AlphaFold2 prediction and reinterpretation of earlier cryo-EM data support a role for the C-terminal tail in stabilizing the TTC5-RNC interaction. This structural model should be considered provisional

until higher-resolution structures are available. Nonetheless, the model explains why deletion of this tail impairs RNC recognition, and identifies this previously overlooked element of TTC5 as a crucial regulatory switch involved in both repression and activation of tubulin mRNA decay.

The ability to control TTC5 activity by αβ-tubulins is of physiological importance. TTC5 mutants that impair αβ-tubulin-mediated sequestration are constitutively active, leading to diminished tubulin mRNA levels and compromised chromosome alignment and segregation during mitosis. These same endpoint phenotypes were also seen in TTC5 and SCAPER knockouts and inactivating mutants, where autoregulation is completely lost and steady-state tubulin mRNA levels are higher than normal[14,15]. This is because mitotic fidelity is extraordinarily sensitive to altered microtubule dynamics and biomechanical properties of the mitotic spindle[43]. Both microtubule stabilization and destabilization cause similar loss of mitotic fidelity[29]. Errors in chromosome alignment and segregation commonly result in aneuploidy and DNA damage[44,45], both of which have been linked to human diseases, such as cancer[46–50].

Mutations in TTC5 and SCAPER have also been implicated in neurodevelopmental disorders[22–27], underscoring the broader importance of tubulin autoregulation in human physiology. Tubulin autoregulation is highly conserved amongst higher eukaryotes, operating in all cell types tested so far[16–18,51–53]. Yet for their proper functioning, differentiated cells require different ratios of soluble vs polymerized αβ-tubulins. Furthermore, this ratio may also need to be adjusted dynamically in response to physiologic context or different stages of the cell cycle. How cells fine-tune the tubulin autoregulation pathway to respond to context- and cell-type-dependent needs remains to be elucidated. Our discovery of αβ-tubulins as a key control point for TTC5 regulation opens the door to unraveling the signals that regulate this step. Analogous regulatory mechanisms may operate on other steps in this pathway including the C-terminal molecular switch element in TTC5, and SCAPER, a known target of cell cycle-regulated kinases[54–56].

Methods
Plasmids and reagents
Tubulin constructs (human TUBB and TUBA1B) for in vitro translation in rabbit reticulocyte lysate (RRL) were cloned into pCDNA3.1. Constructs used for the expression and purification of WT or mutant 6XHis-Twin-Strep-TTC5 recombinant proteins were cloned into the pET28a vector. Mutant *E.coli* tyrosyl-tRNA synthetase for incorporation of Bpa was expressed and purified from the pET21 vector as previously described[57]. *Bacillus stearothermophilus* suppressor tRNA^{Tyr} sequence[58] carrying T7 promoter sequence at 5′ and a BSTN1 restriction site at 3′ was cloned into pRSET. For BiFC experiments, VC-TUBA1B/TUBB-P2A-VN-TTC5 constructs were synthesized by Twist Bioscience (used Venus sequence from Addgene plasmid #105804[59]) and TTC5 mutants generated by site-directed mutagenesis. For a generation of stable cell lines, TTC5 WT or mutants were sub-cloned into the pcDNA 5/FRT/TO vector.

Cell culture
Flp-In T-REx HeLa cells (R71407, Invitrogen) and Flp-In T-REx HEK 293 cells (R78007, Invitrogen) were maintained in DMEM supplemented with 10% fetal bovine serum. Rescue cell lines with stable expression of N-terminally-tagged TurboID-, Flag- or Strep-TTC5 (WT and mutants) were generated from the TTC5 knockout cells using the Flp-In system (K650001 Invitrogen) according to the manufacturer's protocol. Expression of transgene was induced with 200 ng/ml doxycycline for 20–48 h. Colchicine, nocodazole, and combretastatin A4 treatments were performed in standard media at indicated concentrations and time duration.

Recombinant protein and tRNA purification
WT and mutant 6× His-Twin-Strep-tagged TTC5 were purified from *E. coli* (BL21) cells. Briefly, cells were transformed with pET28a plasmid encoding WT or mutant TTC5 and grown at 37 °C in LB containing 50 µg/ml kanamycin. Induction was done with 0.2 mM IPTG at an A600 of 0.6 at 16 °C overnight. For Bpa incorporation at position 194 in TTC5 protein, cells were co-transformed with pET28a plasmid encoding the amber mutant TTC5 and the pEVOL-pBpF plasmid (Addgene plasmid #31190). Cells were grown at 37 °C in LB containing 50 µg/ml kanamycin and 25 µg/ml chloramphenicol and induced with 0.2% L- arabinose at an A600 of 0.3 for 30 min followed by a second induction with 0.2 mM IPTG at an A600 of ~0.6 at 16 °C overnight. The bacterial lysate was prepared by French press in 50 ml cold lysis buffer (500 mM NaCl, 20 mM imidazole, 1 mM PMSF, 1 mM TCEP, and 50 mM HEPES pH 7.4) per 1 l of culture. Clarified bacterial lysates from a 1 l culture were bound to a 1 ml column of HisPur Ni-NTA Spin column (ThermoFisher) by gravity flow. Columns were washed with ~10 column volumes of lysis buffer and eluted with 250 mM imidazole in lysis buffer. The eluate was then bound to a 1 ml column of Streptactin Sepharose® resin (IBA 2-1201-002). After extensive washing with 500 mM NaCl, 1 mM TCEP, and 20 mM HEPES pH 7.4, the bound TTC5 protein was eluted with washing buffer containing 50 mM biotin and dialyzed against dialysis buffer (500 mM NaCl, 1 mM TCEP, and 20 mM HEPES pH 7.4). *E.coli* Bpa tyrosyl-tRNA synthetase was purified via the C-terminal His tag on a Ni-NTA column, desalted by a gel filtration column on FPLC, and concentrated by Amicon Ultra centrifugal filter (Millipore, Z717185-8EA). *B. stearothermophilus* tRNA^{Tyr}, was synthesized by in vitro transcription. The pRSET-based construct was digested with BSTN1, yielding a DNA fragment containing the exact tRNA^{Tyr} sequence under a T7 promoter. 5 ml transcription reaction was carried out with 1.2 mg DNA template, 1 mM spermidine, 5 mM DTT, 0.1% Triton, 5 mM NTPs, 25 µM MgCl$_2$, 20 µg/ml E. *coli* pyrophosphatase, 20 µg/ml T7 polymerase and 125 U Recombinant RNasin (Promega) for 4 h at 37 °C. The reaction product was digested with Turbo DNase (Ambion) and extracted by acid phenol-chloroform extraction to yield purified tRNA.

Western blot
Protein samples were resolved using 12% Tris-Tricine or 10% Bis Tris-based gels followed by transfer to 0.2 mm nitrocellulose membrane (Amersham Cytiva). Primary antibody incubations were performed for 1 h at room temperature or 4 °C overnight. Detection was done using HRP-conjugated secondary antibodies and SuperSignal West Pico Chemiluminescent substrate (Thermo Fisher), or DyLight conjugated antibodies (ThermoFisher) and Odyssey Infrared Imaging System (LI-COR). Expression of N-Flag-tagged WT or mutant TTC5 in rescue cell lines was detected by anti-Flag M2-HRP (Sigma A8592, diluted 1:1000), monoclonal anti-Flag M2 (Sigma F3165, diluted 1:1000), anti-Flag (Sigma F7425, lot 0000131574, diluted 1:2000), or anti-Strep antibody (Abcam ab76949, lot 1072730-2, diluted 1:2000). Ribosomal proteins were detected by anti-RPL8 antibody (Abcam ab169538) or anti-RPS24 antibody (Abcam ab196652), β-tubulin by antibodies (Cell Signaling Technologies 2128, Sigma-Aldrich T7816), α-tubulin by monoclonal antibody (Invitrogen 14-4502-37, clone DM1A, lot 2398350), and GAPDH with anti-GAPDH antibody (ThermoFisher MA515738, clone GA1R, lot YG374752 diluted 1:10 000). TTC5 was detected by using anti-TTC5 antibodies (Epigentek A66330, lot 2211011, diluted 1:1000; Novus Biologicals NBP1-76636, lot 3053-0201, diluted 1:1000; and ProSci 3053, lot 3053-0201, diluted 1:1000). BiFC constructs were detected using a rabbit polyclonal anti-GFP antibody (Torrey Pines Biolabs, TP401, lot 040711, diluted 1:1000).

In vitro transcription and translation
All in vitro transcription of tubulin constructs utilized PCR products as a template. The 5′ primer contains the SP6 promoter sequence and

anneals to the CMV promoter of pCDNA3.1. The 3′ primers anneal at codon 54–60 or 84–90 of nascent tubulin and contain an extra sequence encoding MKLV to generate 64-mer or 94-mer constructs, respectively. Transcription reactions were carried out with SP6 polymerase for 1 h at 37 °C. Transcription reactions were directly used for in vitro translation in a homemade rabbit reticulocyte lysate (RRL)-based translation system in the presence of ^{35}S-methionine as previously described[60]. For incorporation of *p*-benzoyl-L-phenylalanine (Bpa) by amber suppression at position 7 of the nascent tubulin chain, 5 μM *B. Stearothermophilus* tRNA^{Tyr}, 0.25 μM Bpa tyrosyl-tRNA synthetase, and 0.1 mM Bpa were included in the translation reaction as described previously[14]. As indicated in the figure legends, WT or mutant 6XHis-TwinStrep-tagged TTC5 were included in the translation reactions. Translation reactions were performed at 32 °C for 15–20 min. For analysis of the total translation level of nascent chains, a 1 μl aliquot of the translation reaction was mixed with protein sample buffer and analyzed by SDS-PAGE and autoradiography.

In vitro analysis of TTC5 binding to tubulin RNCs

To test the binding of WT or mutant TTC5 variants, 20–40 μl translation reaction of nascent α- or β-tubulin 64-mer containing 100–250 nM WT or mutant 6XHis-Twin-Strep-tagged TTC5 were carried out. The reactions were diluted 10-fold with PSB and incubated with 5 μl Streptactin Sepharose (IBA 2-1201-010) at 4 °C for 2 h. Beads were washed four times with 400 μl PSB and eluted with 20 μl of 50 mM biotin in PSB at 4 °C for 30 min. Eluates were mixed with protein sample buffer for SDS-PAGE and analyzed with SYPRO Ruby protein gel stain (ThermoFisher S12000), autoradiography, or western blotting.

TTC5-RNC UV crosslinking analysis

Crosslinking was performed on isolated RNCs stalled after synthesis of a β-tubulin 94-mer as described previously[14]. Stalling was achieved by using a transcript truncated within the coding region at the desired codon. To isolate the stalled RNCs, 50 μl translation reactions were rapidly cooled on ice and layered on a 200 μl sucrose cushion in physiological salt buffer (PSB: 50 mM Hepes, pH 7.4, 100 mM KAc, 2 mM MgCl$_2$). Centrifugation was in a TLA 120.1 rotor (Beckman) at 436,800 g for 1 h at 4 °C. The ribosome pellets were resuspended in 20 μl PSB on ice. Porcine brain tubulin (Cytoskeleton Inc. #T240) was added to isolated RNCs and incubated for 10 min on ice. The reactions were then placed on ice -10 cm away from a UVP B-100 series lamp (UVP LLC) for 10 min. For analysis of total crosslinking products, 2.5 μl of the reactions were mixed directly with protein sample buffer for SDS-PAGE gel electrophoresis and analyzed by autoradiography. For immunoprecipitation of tubulin nascent chain and endogenous TTC5 crosslinking product, 20 μl of the crosslinking reactions were adjusted to 1% SDS, denatured by heating at 95 °C for 1 min, diluted 10-fold with 180 μl IP buffer (100 mM NaCl, 50 mM Hepes, pH 7.4, 1% Triton X-100) and incubated with 1 μg of TTC5 antibody and 5 μl of protein A agarose at 4 °C for 2 h. Beads were washed three times with 400 μl IP buffer and eluted with protein sample buffer for SDS-PAGE gel electrophoresis and autoradiography.

Autoregulation assay

Parental HeLa T-REx, TTC5 knockout, and indicated rescue cell lines were grown to ~70% confluency in 6-well plates in the presence of 200 ng/ml doxycycline for 24 h. To activate tubulin autoregulation pathway media containing either DMSO (vehicle control) or microtubules destabilizing drug colchicine (1 μM) was added to cells for 7 h. Cells were harvested by scraping in RA1 lysis buffer and total RNA was isolated using the NucleoSpin RNA Mini Kit for RNA Isolation (Macherey-Nagel, 740955) according to the manufacturer's protocol. One microgram of total RNA was used to synthesize cDNA using the SensiFAST cDNA Synthesis Kit (Bioline, BIO-65054) following the manufacturer's instructions. qPCR was carried out using 10 ng of cDNA

and 2× PowerUp SYBR Green master mix (Life Technologies, A25777) and indicated primers on a BioRad thermocycler (BioRad). Data analysis was performed using the ddCt method[61]. All data were normalized to reference housekeeping genes, and to either DMSO-treated controls or parental cell lines as indicated. Experiments include at least three biological replicates. Processing, statistical analysis, and data plotting were performed in R (version 4.4.1). A list of primers used for qPCR is provided in Supplementary Table 1.

Recombinant TTC5 pulldown assays of cell lysates

TTC5 knockout cells were grown to 70–80% confluency in a 145 mm dish and treated with DMSO control, colchicine (10 μM), or nocodazole (10 μM) for the times indicated in the figure legends. For the preparation of cytosolic cell lysates, cells were pelleted by centrifugation at 500 g for 5 min and lysed with lysis buffer (100 mM KAc, 5 mM MgAc$_2$, 1 mM DTT, 100 μg/ml digitonin, 1× EDTA-free protease inhibitor cocktail (Roche) and 50 mM HEPES pH 7.4) for 10 min on ice. Lysates were cleared by centrifugation at 20,000×g for 15 min at 4 °C. Lysate concentrations were determined by Pierce BCA assay kit (ThermoFisher). An aliquot of the lysates was used for total RNA extraction and analyzed for tubulins mRNA by RT-qPCR as described above. Another aliquot of lysate was incubated with 500 nM recombinant TTC5 for 2 min on ice followed by incubation with 10 μl Streptactin Sepharose for 2 h at 4 °C to recover TTC5 and all bound components. Control samples omitted recombinant TTC5. Beads were washed three times with 400 μl PSB and eluted with 50 μl of 50 mM biotin in PSB at 4 °C for 30 min. Eluted samples were analyzed by SDS-PAGE and SYPRO Ruby stain to visualize TTC5 and associated proteins.

Flag- and Strep-TTC5 pulldowns from stable cell lines

To analyze interaction partners of TTC5^{WT} and indicated mutants we used HeLa T-REx TTC5 KO cells expressing either Flag- or Twin-Strep-tagged version of TTC5 under the doxycycline-inducible promoter. Cells were grown in 150 mm plates up to 80–90% confluency in the presence of 200 ng/ml doxycycline for at least 20 h. Cells were washed once with ice-cold PBS, pelleted, and cytosolic extracts were prepared by lysis in 1 ml digitonin lysis buffer for 10 min on ice (50 mM HEPES pH 7.4, 100 mM KAc, 5 mM MgAc$_2$, 1 mM DTT, 1× EDTA-free protease inhibitor cocktail (Roche), 100 μg/ml digitonin). Lysates were cleared by centrifugation at maximum speed at 4 °C for 15 min, followed by a 1-h incubation at 4 °C with 20 μl of either Anti-FLAG M2 Magnetic Beads (Sigma M8823) for Flag-TTC5 cell lines, or MagStrep Strep-Tactin beads (IBA 2-1613) for Twin-Strep-TTC5 cell lines. Beads were then washed four times with physiological salt buffer (PSB: 50 mM HEPES pH 7.4, 100 mM KAc, 2 mM MgCl2, 10 μg/ml digitonin) with a change of tube for the last wash. Elution was done by adding either 20 μl of 0.2 mg/ml of 3xFLAG peptide (Sigma-Aldrich F4799) or 20 μl of 1× Strep-Tactin Elution Buffer (IBA 2-1042-025) to the beads at 4 °C for 30 min. Eluted proteins were separated by SDS-PAGE and analyzed by western blot with indicated antibodies.

Microtubule co-pelleting assay

Five percent glycerol and 1 mM GTP were added to stock porcine tubulin (7 mg/ml) in General Tubulin Buffer (GTB: 2 mM MgCl2, 0.5 mM EGTA, 80 mM PIPES pH 6.9) and incubated at 37 °C for 20 min to assemble microtubules in vitro. Twenty-micromolar taxol was added to stabilize polymerized microtubules after incubation. Recombinant TTC5 was buffered and exchanged into binding buffer (100 mM KCl, 5 mM MgCl2, 1 mM EGTA, and 20 mM HEPES pH 7.4). Two-and-a-half micromolar TTC5 was incubated with 0.6 mg/ml assembled microtubules at room temperature for 30 min. A 50 μl mixture was layered on a 100 μl glycerol cushion (100 mM KCl, 5 mM MgCl2, 1 mM EGTA, 60% Glycerol, 20 μM taxol, and 20 mM HEPES pH 7.4) and centrifuged at 100,000×g at room temperature for 40 min to pellet the microtubules. The supernatant was carefully removed, and

the pellet was resuspended in GTB. Proteins in supernatant and resuspended pellet were analyzed using SDS-PAGE followed by SYPRO Ruby staining.

Measurement of TTC5 and tubulin binding constant
Twenty micromolar recombinant TTC5 was labeled with 22 μM Oregon GreenTM 488 Maleimide (ThermoFisher O6034) in 500 mM NaCl, 1 mM TCEP, and 20 mM HEPES pH 7.4 and incubated on ice for 30 min. Excess dye was removed by the desalting column. Fifty nanomolar labeled TTC5 were mixed with various porcine tubulin concentrations in 250 mM NaCl, 1 mM TCEP, and 20 mM HEPES pH 7.4 and measured with microscale thermophoresis (2bind) to generate a binding curve. Measurements were performed in duplicates.

Bimolecular fluorescence complementation (BiFC) analysis
At day 0, 18000 Flp-In T-REx HeLa cells of the indicated genotypes were seeded in an μ-Plate 96-well plate (ibidi #89626) in the presence of 200 ng/ml doxycycline. After 6 h, the medium was exchanged to DMEM without phenol-red (Thermo Fisher Scientific #21063029) supplemented with 10% fetal bovine serum, 50 nM SiR-DNA (Spirochrome #SC007), and 200 ng/ml doxycycline. Cells were incubated for 16 h prior to imaging. High-throughput live cell imaging was performed in an ImageXpress Micro Confocal automated microscope (Molecular Devices™, wide-field mode) equipped with a 40× water immersion objective (0.95 NA, Nikon). A total of 8–12 regions of interest were acquired per well. Image segmentation was performed using a custom module editor MetaXpress from Molecular Devices. Masks were generated to extract Venus fluorescence intensity across all conditions. Briefly, cell nuclei and body masks were created using SiR-DNA to define a master object (all cells). An automated data analysis pipeline was then applied to identify cells that either express or do not express the constructs based on Venus's fluorescence intensity. Quantitative analysis was carried out only on cells with detectable fluorescence intensity and values were plotted using Graph Pad Prism 8. Statistical analysis was performed using Graph Pad Prism 8, which reports exact p-values to a maximum of four decimal places and all values lower than that as a range (<0.0001).

Proximity labeling in Figs. S1p, q and S2c
HEK T-REx TTC5 KO cells were complemented with TurboID-FLAG-TTC5 constructs expressed from stably integrated pcDNA5/FRT/TO plasmid. For each condition, a 145 mm plate of WT cells or TurboID-TTC5 cells was grown to 70% confluency. To avoid strong overexpression of TurboID-TTC5, leaky expression from the doxycycline-inducible promoter was used without the addition of doxycycline. Cells were treated for 30 min with 10 μM colchicine as indicated and then 50 μM biotin (APExBIO A8010) was added for another 2.5 h. Cells were washed once with ice-cold PBS, pelleted, and cytosolic extracts were prepared by lysis in 0.8 ml digitonin lysis buffer per plate for 10 min on ice (50 mM HEPES pH 7.4, 100 mM KAc, 5 mM MgAc₂, 1 mM DTT, 1x EDTA-free protease inhibitor cocktail (Roche), 0.01% digitonin). Lysates were cleared by centrifugation at 20000 g at 4 °C. Lysates were then incubated on a rotating wheel with 20 μl of streptavidin-coupled magnetic beads (Pierce 88817) for 1.5 h at 4 °C. Beads were then washed with 1 ml each of physiological salt buffer (PSB: 50 mM HEPES pH7.4, 100 mM KAc, 2 mM MgAc₂) with 0.01% digitonin, wash buffer 1 (1% SDS, 10 mM Tris-HCl pH 8), wash buffer 2 (1 M NaCl, 10 mM Tris-HCl pH 8, 0.01% digitonin), and wash buffer 3 (2 M urea, 10 mM Tris-HCl pH 8, 0.01% digitonin), and PSB with 0.01% digitonin. Beads were transferred to a fresh tube with the last wash and eluted with 20 μl sample buffer supplemented with 2 mM biotin for 5 min at 95 °C. Eluted proteins were separated by SDS-PAGE and analyzed by total protein staining with SYPRO Ruby, or by western blot. For mass spectrometry comparison of biotinylated proteins under control (DMSO) and colchicine-treated conditions, we re-analyzed a previously

published dataset of TurboID-TTC5 proteomics data[15]. Samples were prepared as described above with minor modifications and quantified with tandem mass tag-labeling of peptides followed by proteomic analysis as described previously[15]. Mass spectrometry data are accessible via the ProteomeXchange Consortium via the PRIDE partner repository[62] with the dataset identifier PXD041096. Processed data are provided in Supplementary Data 1.

Proximity labeling in Fig. S3g
TurboID-Flag construct was fused to the N-terminus of TTC5 (WT or mutants) and cloned into pcDNA5/FRT/TO vector. HeLa T-REx TTC5 KO cell line was used to create rescue (WT) or indicated mutant cell lines with stable expression of TurboID-Flag-TTC5. For western blot of biotinylated proteins cells were seeded at 70% confluency and induced with 5 ng/ml doxycycline for 24 h. Fifty-micromolar biotin was added to cells for 15 min at 37 °C followed by five washes with ice-cold PBS and cell lysis with RIPA buffer (50 mM Tris HCl pH 8, 150 mM NaCl, 1% Triton X-100, 0.5% sodium deoxycholate, 0.1% SDS). Total protein concentration was measured with Pierce BCA Protein Assay Kit (Thermo Scientific 23227) and 15 μg of total protein lysates were analyzed by western blot. Biotynylated proteins were visualized with Streptavidin conjugated to horseradish peroxidase (Invitrogen S911). The experiment was performed in four biological replicates. Quantification of tubulin biotinylation was done using Fiji. The signal intensity of biotinylated tubulin and TurboID-TTC5 bands was measured to calculate the tubulin/TTC5-TurboID ratio for each cell line. TTC5 knockout cells were used as background control and the TurboID-TTC5 WT sample served as a reference (100% of biotinylated tubulin) to normalize data of TTC5 mutants.

High-resolution separation of tubulin subunits in Fig. S1e, f
For Fig. S1e, HEK T-REx TTC5 KO cells were complemented with Strep-TTC5 expressed from transiently transfected pcDNA5/FRT/TO plasmid. Expression of Strep-TTC5 was induced by the addition of doxycycline (1 μg/ml) for 24 h. Cells were washed once with ice-cold PBS, pelleted, and cytosolic extracts were prepared by lysis in 0.2 ml digitonin lysis buffer per 100 mm plate for 10 min on ice (50 mM HEPES pH 7.4, 100 mM KAc, 5 mM MgAc₂, 1 mM DTT, 1x EDTA-free protease inhibitor cocktail (Roche), 0.01% digitonin). Lysates were cleared by centrifugation at 20,000×g for 5 min at 4 °C. For Fig. S1f, 0.5 μM recombinant Strep-TTC5 was mixed with 0.5 μM porcine brain tubulin in PSB on ice for 10 min. Cleared lysates (Fig. S1e) or 200 μl mixtures of strep-TTC5 and porcine tubulin (Fig. S1f) were incubated on a rotating wheel with 10 μl of Strep-Tactin agarose beads (IBA 6-6350-025) for 2 h at 4 °C. Beads were washed four times with physiological salt buffer (PSB: 50 mM HEPES pH 7.4, 100 mM KAc, 2 mM MgCl2, 10 μg/ml digitonin) with a change of tube for the last wash. Elution was done by adding 20 μl of 25 mM biotin in PSB to the beads at 4 °C for 30 min. Eluted proteins were separated by a 7.5% resolving gel that allows a high-resolution separation of tubulin subunits as previously described[63]. The gels were run in a 1× running buffer (0.1% SDS, 192 mM glycine, and 25 mM Tris-HCl pH 8.8) at 120 V for 90 min and analyzed by Sypro Ruby staining or western blot with indicated antibodies.

Analysis of TTC5 interaction partners by proteomics
To analyze in vivo interaction partners of TTC5 before and after colchicine treatment, we used 293 T-REx TTC5 KO cells complemented with doxycycline-inducible EGFP-tagged TTC5 as previously described in ref. 15. EGFP-TTC5 was induced by doxycycline (1 μg/ml for 24 h) and cells were grown in 145 mm plates to around 80% confluence and treated with 10 μM colchicine for 0 min, 15 min, 30 min, 60 min, 120 min, or 180 min. Cells were washed once in ice-cold PBS, pelleted, and cytosolic extracts were prepared by lysis in 1 ml digitonin lysis buffer per plate for 10 min on ice (50 mM HEPES pH 7.4, 100 mM KAc,

5 mM MgAc₂, 1 mM DTT, 1× EDTA-free protease inhibitor cocktail (Roche), 0.01% digitonin). Lysates were cleared by centrifugation at maximum speed at 4 °C in a table-top centrifuge. Lysates were then incubated on a rotating wheel with 10 µl of GFP-trap agarose (ChromoTek) for 1 h at 4 °C. Beads were then washed twice with 1 ml each of physiological salt buffer containing 0.01% digitonin, and twice with physiological salt buffer without detergent. For each of the six-time points, one biological replicate was analyzed, for which three technical replicates were subjected to label-free quantification by LC-MS/MS (18 samples in total). The bead samples were buffer exchanged twice with 100 mM ammonium bicarbonate and on the last wash, beads were left with minimum buffer to cover. The cysteines were reduced by adding 30 µL of 10 mM DTT and then alkylated with 30 uL of 55 mM iodoacetamide. Proteins were digested on beads with 1 µg trypsin (Promega, UK) for 18 h at 37 °C. Peptides were acidified with the addition of 4 µl formic acid 2% (v/v). The bead/peptide mix was then centrifuged at 14,000×g for 5 min and the 20 µl of supernatant was placed into a vial for LC-MS/MS analysis. LC-MS/MS was performed on an Ultimate U3000 HPLC (ThermoFisher Scientific, San Jose, USA) hyphenated to an Orbitrap QExactive Classic mass spectrometer (ThermoFisher Scientific, San Jose, USA). Peptides were trapped on a C18 Acclaim PepMap 100 (5 µm, 300 µm × 5 mm) trap column (ThermoFisher Scientific, San Jose, USA) and eluted onto a C18 Acclaim PepMap100 3 µm, 75 µm × 250 mm (ThermoScientific Dionex, San Jose, USA) using 30 min gradient of acetonitrile (4–30%). For data-dependent acquisition, MS1 scans were acquired at a resolution of 35,000 (AGC target of 1e6 ions with a maximum injection time of 50 ms) followed by ten MS2 scans acquired at a resolution of 17,500 (AGC target of 2e5 ions with a maximum injection time of 100 ms) using a collision-induced dissociation energy of 25. Dynamic exclusion of fragmented m/z values was set to 30 s. Raw data were imported and processed in MASCOT (Matrix Science). The raw files were submitted to a database search against the UniProt/SwissProt database. Database search parameters were set with a precursor tolerance of 10 ppm and a fragment ion mass tolerance of 0.8 Da. One missed enzyme cleavage was allowed and variable modifications for oxidized methionine, carbamidomethyl, and phospho STY were included. The acquired LC-MS/MS raw files were processed using MaxQuant[64] with the integrated Andromeda search engine (v1.6.6.0), and searched against the Human Reviewed UniProt Fasta database (2019). The MaxQuant output file (proteinGroups.txt) was then processed with Perseus software (v1.6.10.45)[65]. After uploading the matrix, the data was filtered to remove identifications from the reverse database, identifications with modified peptides only, and common contaminants. Data were log2-transformed, a valid value filter was applied and missing values for remaining proteins were imputed with standard settings. We found that the 0- and 15-min timepoints showed very similar interaction profiles and were thus grouped as "untreated control" samples, and the 60-, 120-, and 180-min timepoints showed highly similar profiles and were grouped as "colchicine-treated" samples for further analysis. One replicate of the 180-min timepoint was identified as an outlier using principal component analysis and discarded from further analysis. The 30-min timepoint showed an intermediate profile and was omitted for this analysis. To generate a volcano plot we compared all samples in the "untreated control" vs "colchicine-treated" groups. A two-sided Student's t-test was performed for statistical analysis, and no correction for multiple comparisons was applied. The mass spectrometry proteomics data have been deposited to the ProteomeXchange Consortium via the PRIDE partner repository[62] with the dataset identifier PXD050557. Processed data are provided in Supplementary Data 2.

Hydrogen–deuterium exchange mass spectrometry (HDX-MS)

HDX-MS was performed at the UniGe Protein Platform (University of Geneva, Switzerland) following a well-established protocol with minimal modifications[66]. Details of reaction conditions are provided in Supplementary Table 2.

HDX reactions were done in 50 µl volumes with a final protein concentration of 1.6 µM TTC5 and a 1.5-fold molar excess of αβ-tubulins. Briefly, 78 picomoles of protein were pre-incubated with αβ-tubulins or buffer for 1 h on ice in a final volume of 3 µl before deuteration. The deuterium on-exchange reaction was initiated by adding 47 µl of D2O exchange buffer (20 mM HEPES pH 7.5/150 mM NaCl/1 mM TCEP in D2O) to the protein-ligand mixture. Reactions were carried out on ice for three incubation times (3 s, 30 s, and 300 s) and terminated by the sequential addition of 20 µl of ice-cold quench buffer (4 M Gdn-HCl/1 M NaCl/0.1 M NaH₂PO₄ pH 2.5/1% Formic Acid). The 3-s deuteration is estimated by counting the up-and-down-pipetting cycles in lieu of a timer. Samples were immediately frozen in liquid nitrogen and stored at −80 °C for up to two weeks. All experiments were repeated in triplicates. To quantify deuterium uptake into the protein, samples were thawed and injected in a UPLC system immersed in ice with 0.1% FA as the liquid phase. The protein was digested via two immobilized pepsin columns (Thermo #23131), and peptides were collected onto a VanGuard precolumn trap (Waters). The trap was subsequently eluted, and peptides separated with a C18, 300 Å, 1.7 µm particle size Fortis Bio 100 ×2.1 mm column over a gradient of 8–30% buffer C over 20 min at 150 ml/min (Buffer B: 0.1% formic acid; buffer C: 100% acetonitrile). Mass spectra were acquired on an Orbitrap Velos Pro (Thermo), for ions from 400 m/z to 2200 m/z using an electrospray ionization source operated at 300 °C, 5 kV of ion spray voltage. Peptides were identified by data-dependent acquisition of a non-deuterated sample after MS/ MS and data were analyzed by Mascot. All peptides analyzed are shown in Supplementary Data 3. Deuterium incorporation levels were quantified using HD examiner software version 3.3 (Sierra Analytics), and the quality of every peptide was checked manually. Results are presented as a percentage of maximal deuteration compared to the theoretical maximal deuteration level. Changes in deuteration level between two states were considered significant if >12% and >1.4 Da and p < 0.01 (unpaired t-test) for a single deuteration time. The mass spectrometry proteomics data have been deposited to the ProteomeXchange Consortium via the PRIDE partner repository[62] with the dataset identifier PXD050483.

Multiple sequence alignment (MSA) analysis

MSA of TTC5 protein was done using the ConSurf server[35] (server for the identification of functional regions in proteins, https://consurf.tau.ac.il/consurf_index.php). Alignment was performed for the AlphaFold2 predicted model of human TTC5 (AF-Q8N0Z6-F1). Exposed and buried residues of TTC5 were predicted with the NACSES algorithm of ConSurf[67].

Structural modeling

Structure predictions were performed with AlphaFold2 through a local installation of Colabfold 1.2.0[68] using MMseqs2[69] for homology searches and AlphaFold2 multimer[70] for the predictions of single or multiple chains, respectively. To generate figures displaying the predicted interaction between the TTC5 C-terminus and TUBB/TUBA1B N-terminus, ten predictions for TTC5 with the TUBB or TUBA1B 20 N-terminal amino acids were overlaid. The top-ranked model for the TTC5-TUBB interaction was docked into the cryo-EM density map of a recent structure (PDB: 8BPO) as described in ref. 15.

Live cell imaging and data analysis

Flp-In T-REx HeLa cells of the genotypes indicated in the figure legends were plated in 8-well Lab Tek II Chamber 1.5 German coverglass dishes (Thermo Fisher 155409) in regular growth medium, and incubated for 6 h. The medium was then changed to Leibovitz's L-15 without phenol-red (ThermoFisher, 21083027) supplemented

with 10% fetal bovine serum, 200 ng/ml doxycycline and 50 nM SiR-DNA (Cytoskeleton CY-SC007). Cells were incubated for 24 h prior to imaging. Time-lapse images were acquired using a Nikon Eclipse Ti2-E inverted microscope (Nikon), equipped with a Kinetix sCMOS camera (Photometrics), Spectrax Chroma light engine for fluorescence illumination (Lumencor), a perfect focus system, and an incubation chamber with 37 °C and controlled humidity (OkoLab). Three-dimensional images at multiple stage positions were acquired in steps of 2 µm, every 7 min for 10 h using NIS Elements (Nikon) and 20× Plan Apochromat Lambda objective (NA 0.80, Nikon). Maximum intensity projections and inverted color profiles of representative examples of mitoses were prepared in Fiji (ImageJ, version 2.14.0/1.54f) and exported as still images. Analysis of mitotic cells was performed using 3D reconstructions in Fiji. The parameters scored (based on the SiR-DNA signal) were the occurrence of unaligned chromosomes in metaphase, and chromosome segregation errors in anaphase. Analyses of at least 100 cells per cell line in three biological replicates were documented using Excel and processed and plotted using R (version 4.4.1). Statistical analyses were performed in R. Instances where not all the chromosomes were properly aligned on the spindle equator in metaphase and/or anaphase are classified as chromosome alignment errors. Instances where sister chromatids failed to properly separate, either segregating both into the same daughter cell or forming a bridge in anaphase were classified as segregation errors. Numbers reported represent the percentage of cells experiencing either abnormality.

Statistics and reproducibility

For all the data presented in the main figures, statistical tests with exact *p*-values derived, the number of independent biological replicates, and where applicable number of analyzed cells are provided in the figures and figure legends. For all the data presented in the Supplementary Figures, statistical tests with exact *p*-values derived, number of independent biological replicates, and where applicable number of analyzed cells are provided in the figure legends and Source Data file. No statistical method was used to predetermine the sample size. "No data were excluded from the analyses"; "The experiments were not randomized"; and "The Investigators were not blinded to allocation during experiments and outcome assessment".

Reporting summary

Further information on research design is available in the Nature Portfolio Reporting Summary linked to this article.

Data availability

The HDX-MS proteomics data have been deposited to the ProteomeXchange Consortium via the PRIDE repository with the dataset identifier PXD050483. The mass spectrometry proteomics data of eGFP-TTC5 interactome have been deposited to the ProteomeXchange Consortium via the PRIDE partner repository with the dataset identifier PXD050557. Source data are provided with this paper.

References

1. Wade, R. H. & Hyman, A. A. Microtubule structure and dynamics. *Curr. Opin. Cell Biol.* **9**, 12–17 (1997).
2. Muroyama, A. & Lechler, T. Microtubule organization, dynamics and functions in differentiated cells. *Development* **144**, 3012–3021 (2017).
3. Gasic, I. & Mitchison, T. J. Autoregulation and repair in microtubule homeostasis. *Curr. Opin. Cell Biol.* **56**, 80–87 (2019).
4. Mitchison, T. & Kirschner, M. Dynamic instability of microtubule growth. *Nature* **312**, 237–242 (1984).
5. Goodson, H. V. & Jonasson, E. M. Microtubules and microtubule-associated proteins. *Cold Spring Harb. Perspect. Biol.* **10**, a022608 (2018).
6. Wieczorek, M., Bechstedt, S., Chaaban, S. & Brouhard, G. J. Microtubule-associated proteins control the kinetics of microtubule nucleation. *Nat. Cell Biol.* **17**, 907–916 (2015).
7. Zheng, Y., Wong, M. L., Alberts, B. & Mitchison, T. Nucleation of microtubule assembly by a gamma-tubulin-containing ring complex. *Nature* **378**, 578–583 (1995).
8. Geel, O. V., Cheung, S. & Gadella, T. W. J. Combining optogenetics with sensitive FRET imaging to monitor local microtubule manipulations. *Sci. Rep.* **10**, 6034 (2020).
9. Cleveland, D. W., Lopata, M. A., Sherline, P. & Kirschner, M. W. Unpolymerized tubulin modulates the level of tubulin mRNAs. *Cell* **25**, 537–546 (1981).
10. Ben-Ze'ev, A., Farmer, S. R. & Penman, S. Mechanisms of regulating tubulin synthesis in cultured mammalian cells. *Cell* **17**, 319–325 (1979).
11. Theodorakis, N. G. & Cleveland, D. W. Physical evidence for cotranslational regulation of beta-tubulin mRNA degradation. *Mol. Cell Biol.* **12**, 791–799 (1992).
12. Yen, T. J., Machlin, P. S. & Cleveland, D. W. Autoregulated instability of beta-tubulin mRNAs by recognition of the nascent amino terminus of beta-tubulin. *Nature* **334**, 580–585 (1988).
13. Yen, T. J., Gay, D. A., Pachter, J. S. & Cleveland, D. W. Autoregulated changes in stability of polyribosome-bound beta-tubulin mRNAs are specified by the first 13 translated nucleotides. *Mol. Cell Biol.* **8**, 1224–1235 (1988).
14. Lin, Z. et al. TTC5 mediates autoregulation of tubulin via mRNA degradation. *Science* **367**, 100–104 (2020).
15. Höpfler, M. et al. Mechanism of ribosome-associated mRNA degradation during tubulin autoregulation. *Mol. Cell* **83**, 2290–2302.e13 (2023).
16. Gasic, I., Boswell, S. A. & Mitchison, T. J. Tubulin mRNA stability is sensitive to change in microtubule dynamics caused by multiple physiological and toxic cues. *PLoS Biol.* **17**, e3000225 (2019).
17. Phyo, S. A. et al. Transcriptional, post-transcriptional, and post-translational mechanisms rewrite the tubulin code during cardiac hypertrophy and failure. *Front. Cell Dev. Biol.* **10**, 837486 (2022).
18. Caron, J. M., Jones, A. L. & Kirschner, M. W. Autoregulation of tubulin synthesis in hepatocytes and fibroblasts. *J. Cell Biol.* **101**, 1763–1772 (1985).
19. Magiera, M. M. & Janke, C. Post-translational modifications of tubulin. *Curr. Biol.* **24**, R351–R354 (2014).
20. Bheda, A., Gullapalli, A., Caplow, M., Pagano, J. S. & Shackelford, J. Ubiquitin editing enzyme UCH L1 and microtubule dynamics: implication in mitosis. *Cell Cycle* **9**, 980–994 (2010).
21. Ren, Y., Zhao, J. & Feng, J. Parkin binds to α/β tubulin and increases their ubiquitination and degradation. *J. Neurosci.* **23**, 3326–3324 (2003).
22. Musante, L. et al. TTC5 syndrome: clinical and molecular spectrum of a severe and recognizable condition. *Am. J. Med. Genet. A* **188** 1–14 (2022).
23. Rasheed, A. et al. Bi-allelic TTC5 variants cause delayed developmental milestones and intellectual disability. *J. Med. Genet.* **58**, 237–246 (2021).
24. Miyamoto, S. et al. A boy with biallelic frameshift variants in TTC5 and brain malformation resembling tubulinopathies. *J. Hum. Genet.* **66**, 1189–1192 (2021).
25. Fasham, J. et al. Delineating the expanding phenotype associated with SCAPER gene mutation. *Am. J. Med. Genet. A* **179**, 1665–1671 (2019).
26. Kahrizi, K. et al. Homozygous variants in the gene SCAPER cause syndromic intellectual disability. *Am. J. Med. Genet. A* **179**, 1214–1225 (2019).
27. Tatour, Y. et al. Mutations in SCAPER cause autosomal recessive retinitis pigmentosa with intellectual disability. *J. Med. Genet.* **54**, 698 (2017).

28. Bakhoum, S. F., Genovese, G. & Compton, D. A. Deviant kinetochore microtubule dynamics underlie chromosomal instability. *Curr. Biol.* **19**, 1937–1942 (2009).

29. Bakhoum, S. F., Thompson, S. L., Manning, A. L. & Compton, D. A. Genome stability is ensured by temporal control of kinetochore–microtubule dynamics. *Nat. Cell Biol.* **11**, 27–35 (2009).

30. Tilney, L. G. & Porter, K. R. Studies on the microtubules in heliozoa. II. The effect of low temperature on these structures in the formation and maintenance of the axopodia. *J. Cell Biol.* **34**, 327–343 (1967).

31. Weber, K., Pollack, R. & Bibring, T. Antibody against tuberlin: the specific visualization of cytoplasmic microtubules in tissue culture cells. *Proc. Natl. Acad. Sci. USA* **72**, 459–463 (1975).

32. James, E. I., Murphree, T. A., Vorauer, C., Engen, J. R. & Guttman, M. Advances in hydrogen/deuterium exchange mass spectrometry and the pursuit of challenging biological systems. *Chem. Rev.* **122**, 7562–7623 (2022).

33. Tunyasuvunakool, K. et al. Highly accurate protein structure prediction for the human proteome. *Nature* **596**, 590–596 (2021).

34. Nogales, E., Wolf, S. G. & Downing, K. H. Visualizing the secondary structure of tubulin: three-dimensional map at 4 Å. *J. Struct. Biol.* **118**, 119–127 (1997).

35. Yariv, B. et al. Using evolutionary data to make sense of macromolecules with a "face-lifted" ConSurf. *Protein Sci.* **32**, e4582 (2023).

36. Kerppola, T. K. Design and implementation of bimolecular fluorescence complementation (BiFC) assays for the visualization of protein interactions in living cells. *Nat. Protoc.* **1**, 1278–1286 (2006).

37. Shyu, Y. J., Liu, H., Deng, X. & Hu, C.-D. Identification of new fluorescent protein fragments for bimolecular fluorescence complementation analysis under physiological conditions. *Biotechniques* **40**, 61–66 (2006).

38. Tak, H. et al. Bimolecular fluorescence complementation; lighting-up tau-tau interaction in living cells. *PLoS One* **8**, e81682 (2013).

39. Gay, D. A., Yen, T. J., Lau, J. T. Y. & Cleveland, D. W. Sequences that confer β-tubulin autoregulation through modulated mRNA stability reside within exon 1 of a β-tubulin mRNA. *Cell* **50**, 671–679 (1987).

40. Bachurski, C. J., Theodorakis, N. G., Coulson, R. M. & Cleveland, D. W. An amino-terminal tetrapeptide specifies cotranslational degradation of beta-tubulin but not alpha-tubulin mRNAs. *Mol. Cell Biol.* **14**, 4076–4086 (1994).

41. Gasic, I. Regulation of tubulin gene expression: from isotype identity to functional specialization. *Front. Cell Dev. Biol.* **10**, 898076 (2022).

42. Gadadhar, S., Bodakuntla, S., Natarajan, K. & Janke, C. The tubulin code at a glance. *J. Cell Sci.* **130**, 1347–1353 (2017).

43. Kline-Smith, S. L. & Walczak, C. E. Mitotic spindle assembly and chromosome segregation: refocusing on microtubule dynamics. *Mol. Cell* **15**, 317–327 (2004).

44. Janssen, A., van der Burg, M., Szuhai, K., Kops, G. J. P. L. & Medema, R. H. Chromosome segregation errors as a cause of DNA damage and structural chromosome aberrations. *Science* **333**, 1895–1898 (2011).

45. Bakhoum, S. F. et al. The mitotic origin of chromosomal instability. *Curr. Biol.* **24**, R148–R149 (2014).

46. Cimini, D. Merotelic kinetochore orientation, aneuploidy, and cancer. *Biochim. Biophys. Acta* **1786**, 32–40 (2008).

47. Replogle, J. M. et al. Aneuploidy increases resistance to chemotherapeutics by antagonizing cell division. *PNAS* **117**, 30566–30576 (2020).

48. Rajagopalan, H. & Lengauer, C. Aneuploidy and cancer. *Nature* **432**, 338–341 (2004).

49. Weaver, B. A. A., Silk, A. D., Montagna, C., Verdier-Pinard, P. & Cleveland, D. W. Aneuploidy acts both oncogenically and as a tumor suppressor. *Cancer Cell* **11**, 25–36 (2007).

50. Levine, M. S. & Holland, A. J. The impact of mitotic errors on cell proliferation and tumorigenesis. *Genes Dev.* **32**, 620–638 (2018).

51. Fellous, A., Ginzburg, I. & Littauer, U. Z. Modulation of tubulin mRNA levels by interferon in human lymphoblastoid cells. *EMBO J.* **1**, 835–839 (1982).

52. Pittenger, M. F. & Cleveland, D. W. Retention of autoregulatory control of tubulin synthesis in cytoplasts: demonstration of a cytoplasmic mechanism that regulates the level of tubulin expression. *J. Cell Biol.* **101**, 1941–1952 (1985).

53. Lau, J. T. Y., Pittenger, M. F., Havercroft, J. C. & Cleveland, D. W. Reconstruction of tubulin gene regulation in cultured mammalian cells. *Ann. NY Acad. Sci.* **466**, 75–88 (1986).

54. Tsang, W. Y., Wang, L., Chen, Z., Sánchez, I. & Dynlacht, B. D. SCAPER, a novel cyclin A-interacting protein that regulates cell cycle progression. *JCB* **178**, 621–633 (2007).

55. Williams, R. SCAPER speeds and slows the cell cycle. *J. Cell Biol.* **178**, 543–543 (2007).

56. Tsang, W. Y. & Dynlacht, B. D. Double identity of SCAPER: a substrate and regulator of cyclin A/Cdk2. *Cell Cycle Georget. Tex.* **7**, 702–705 (2008).

57. Chin, J. W. et al. An expanded eukaryotic genetic code. *Science* **301**, 964–967 (2003).

58. Sakamoto, K. et al. Site-specific incorporation of an unnatural amino acid into proteins in mammalian cells. *Nucleic Acids Res.* **30**, 4692–4699 (2002).

59. Szczesny, R. J. et al. Versatile approach for functional analysis of human proteins and efficient stable cell line generation using FLP-mediated recombination system. *PLoS One* **13**, e0194887 (2018).

60. Sharma, A., Mariappan, M., Appathurai, S. & Hegde, R. S. Protein secretion, methods and protocols. *Methods Mol. Biol.* **619**, 339–363 (2010).

61. Livak, K. J. & Schmittgen, T. D. Analysis of relative gene expression data using real-time quantitative PCR and the $2^{-\Delta\Delta CT}$ method. *Methods* **25**, 402–408 (2001).

62. Perez-Riverol, Y. et al. The PRIDE database resources in 2022: a hub for mass spectrometry-based proteomics evidences. *Nucleic Acids Res,* **50**, D543–D552 (2021).

63. Banerjee, A., Bovenzi, F. A. & Bane, S. L. High-resolution separation of tubulin monomers on polyacrylamide minigels. *Anal. Biochem.* **402**, 194–196 (2010).

64. Cox, J. & Mann, M. MaxQuant enables high peptide identification rates, individualized p.p.b.-range mass accuracies and proteome-wide protein quantification. *Nat. Biotechnol.* **26**, 1367–1372 (2008).

65. Tyanova, S. et al. The Perseus computational platform for comprehensive analysis of (prote)omics data. *Nat. Methods* **13**, 731–740 (2016).

66. Wang, H. et al. Autoregulation of class II alpha PI3K activity by its lipid-binding PX-C2 domain module. *Mol. Cell* **71**, 343–351.e4 (2018).

67. Landau, M. et al. ConSurf 2005: the projection of evolutionary conservation scores of residues on protein structures. *Nucleic Acids Res.* **33**, W299–W302 (2005).

68. Mirdita, M. et al. ColabFold: making protein folding accessible to all. *Nat. Methods* **19**, 679–682 (2022).

69. Mirdita, M., Steinegger, M. & Söding, J. MMseqs2 desktop and local web server app for fast, interactive sequence searches. *Bioinformatics* **35**, 2856–2858 (2019).

70. Evans, R. et al. Protein complex prediction with Alphafold-multimer. *bioRxiv* 2021.10.04.463034 (2022).

Acknowledgements

Author contributions

A.B., D.T.E.J, and M.H. co-discovered the C-terminal domain of TTC5 as a molecular switch in tubulin autoregulation. A.B characterized αβ-tubulin/TTC5 complex, generated and tested all the TTC5 mutant cell lines, and identified and characterized binding-deficient mutants (Figs. 2h, i and 3b, h; and S2d and S3a, b, g, j). D.T.E.J. performed proximity labeling with C-terminal truncation mutants of TTC5 (Fig. S2c). M.H. performed in vitro translation assays, GFP-TTC5 and TurboID-TTC5 proteomics experiments, and AlphaFold predictions (Figs. 1g, 2j, and 3f; and S1k, l, O, p, q, S2e, f, and S3h). A.C.A. designed and generated the BiFC assays and performed the related experiments, as well as some RNA measurements (Figs. 3d, e, and g; and S1d, S3d, e, f, and i). O.V. generated and analyzed HDX-MS data (Figs. 2b, e and S2a, b). E.V. purified the recombinant TTC5 proteins and performed some western blots (Figs. S1a, c and S4c). Z.L. discovered αβ-tubulins as repressors of TTC5 while he was a postdoctoral fellow with R.S.H (Figs. 1b–e and S1e–h, m lower). I.G. designed and performed some pulldowns and RNA measurements, microscopy of GFP-TTC5, and phenotypic analysis of mitosis (Figs. 1a, f, 2a, c, d, f, g, k, 3a, c, and 4a–d; and S1b, i–j, m upper, n, S2g, S3c, and S4a–b). I.G., Z.L., and R.S.H. supervised different parts of the project. I.G. conceived the project with input from R.S.H. and M.H., oversaw its implementation, and wrote the manuscript. All authors contributed to manuscript editing.

Competing interests

The authors declare no competing interests.

Additional information

Supplementary information The online version contains supplementary material available at https://doi.org/10.1038/s41467-024-54036-0.

Correspondence and requests for materials should be addressed to Zhewang Lin or Ivana Gasic.

Peer review information *Nature Communications* thanks Hui Xiao, and the other, anonymous, reviewer(s) for their contribution to the peer review of this work. A peer review file is available.

Reprints and permissions information is available at http://www.nature.com/reprints

Publisher's note Springer Nature remains neutral with regard to jurisdictional claims in published maps and institutional affiliations.